

Unsupervised Structured Noise Removal with Variational Lossy Autoencoder

Benjamin Salmon and Alexander Krull

School of Computer, University of Birmingham, Birmingham B15 2TT, UK

brs209@student.bham.ac.uk, a.f.f.krull@bham.ac.uk

Abstract

Most unsupervised denoising methods are based on the assumption that imaging noise is either pixel-independent, i.e., spatially uncorrelated, or signal-independent, i.e., purely additive. However, in practice many imaging setups, especially in microscopy, suffer from a combination of signal-dependent noise (e.g. Poisson shot noise) and axis-aligned correlated noise (e.g. stripe shaped scanning or readout artifacts). In this paper, we present the first unsupervised deep learning-based denoiser that can remove this type of noise without access to any clean images or a noise model. Unlike self-supervised techniques, our method does not rely on removing pixels by masking or subsampling so can utilize all available information. We implement a Variational Autoencoder (VAE) with a specially designed autoregressive decoder capable of modelling the noise component of an image but incapable of independently modelling the underlying clean signal component. As a consequence, our VAE’s encoder learns to encode only underlying clean signal content and to discard imaging noise. We also propose an additional decoder for mapping the encoder’s latent variables back into image space, thereby sampling denoised images. Experimental results demonstrate that our approach surpasses existing methods for self- and unsupervised image denoising while being robust with respect to the size of the autoregressive receptive field. Code for this project can be found at <https://github.com/krulllab/DVLAE>.

1. Introduction

Imaging is usually accompanied by a certain degree of noise which must be removed as a common preprocessing step for many applications. This is especially true in scientific imaging where technology is pushed to the boundary of what is possible. Over the years, a variety of denoising approaches have been devised [17], ranging from traditional filter-based methods [5] to supervised machine learning-based methods [34]. Recently, self- and unsupervised methods (e.g. [2, 14, 23, 24]) were introduced. These

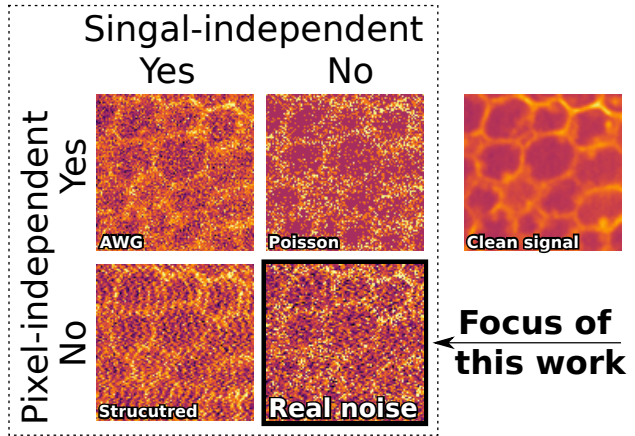


Figure 1. Imaging noise is often assumed to be pixel-independent or signal-independent, which greatly facilitates self/unsupervised denoising. Unfortunately, real noise in many applications is neither. We present an unsupervised denoising approach for this challenging scenario.

methods can be trained directly on the data that is to be denoised and do not require the recording of designated training data. As a result, such approaches have substantially improved the practical applicability of denoising in scientific imaging.

Self- and unsupervised methods separate the imaging noise from the underlying signal by making assumptions about the noise’s statistical nature. These are typically (i) pixel-independence or (ii) signal-independence (Figure 1).

In a pixel-independent (i) noise model, the probability of a noisy recorded image \mathbf{x} given an underlying clean image \mathbf{s} can be described as the product

$$p(\mathbf{x}|\mathbf{s}) = \prod_{i=1}^D p(x_i|s_i), \quad (1)$$

over pixels i . Here, s_i and x_i correspond to the clean signal and noisy measurement at pixel i , and D is the number of pixels in the image. This noise model is assumed by, e.g., [10, 14, 15, 24, 26].

In a signal-independent (*ii*) noise model, the probability distribution of noise is independent of the underlying signal (e.g. [27]). In other words, if the noise $\mathbf{n} = \mathbf{x} - \mathbf{s}$ is defined as the difference between the noisy recorded image \mathbf{x} and the clean signal \mathbf{s} ,

$$p(\mathbf{n}|\mathbf{s}) = p(\mathbf{n}). \quad (2)$$

This noise model is assumed by, e.g., [27, 36]

Unfortunately, signal independence is not a realistic assumption for many practical applications, such as low light microscopy, which are often heavily affected by Poisson shot noise—a consequence of the particle nature of light [17]. A more realistic model frequently used in fluorescence microscopy (e.g. [38]) assumes a combination of Poisson shot noise and Gaussian read-out noise (a consequence of the detector’s electronics).

Additionally, the assumption of pixel independence is often broken and images can suffer from structured noise patterns [1], often in the form of stripe-shaped scanning, read-out or amplification artifacts. Until recently, removing such artifacts required either supervised training with specifically collected data [34], specialized methods that are only applicable in specific cases [12, 20, 31], or involve masking larger areas in the image during training, leading to increased loss of information [3, 35].

In this paper, we present the first unsupervised VAE-based denoiser capable of removing signal-dependent noise that is correlated along rows or columns of the image, as it commonly occurs in real microscopy data. The approach is illustrated in Figure 2. Our method requires neither examples of noise free images, which can be impossible to obtain (e.g. [32]), nor pre-trained noise models [15, 24, 27] or hand-crafted priors [5, 7, 32]. Furthermore, we do not rely on self-supervised denoising techniques, such as pixel masking [3] or subsampling [10], which degrade input image quality and therefore limit denoising performance.

Our approach is based on the findings of Chen *et al.* [4], who investigated the division of labour between a VAE’s latent variable and its autoregressive (AR) decoder as they are trained together to model a data distribution. They found that the autoregressive decoder will generally model all aspects of the distribution it has the capacity to model. The latent variables will then not represent these aspects, instead expressing only what the decoder could not independently model.

We take advantage of this behaviour by designing a decoder that is capable of modelling exactly what we want to be excluded from our latent variables—the imaging noise—while being incapable of modelling the remainder of the data. Specifically, we use an autoregressive (AR) decoder that can only model axis-aligned structures because its receptive field spans only a row or column of the image.

Since structured noise artifacts in microscopy are often axis-aligned, this trains our model to exclude real-life structured noise from the latent variable.

We then propose a second network, termed *signal decoder*, that is trained to map these latent variables back into image space thereby producing denoised images. Relying on Lehtinen *et al.* [19], who showed that noisy images can be used as training targets for denoisers, we train the signal decoder alongside the VAE by using the original noisy data as training target.

To summarise, our main contributions are:

- We demonstrate that an AR decoder with a 1-dimensional receptive field is incapable of modeling natural signals, but is capable of modeling common forms of structured noise in microscopy.
- We introduce a novel architecture using a signal decoder that is trained in a second step to predict the signal from our latent variable.
- We present a novel unsupervised denoising method that can be readily applied without additional training data, relying neither on a signal- nor pixel-independence, outperforming previous self- and unsupervised methods.

2. Related Work

2.1. Self-supervised denoising

Self-supervised methods use a noisy image as its own training target. To prevent the network from learning the identity function, the image is corrupted in some way. One technique [2, 14, 18, 33, 35] introduces blind-spots, forcing a network to predict a pixel’s value from surrounding pixels. Another trains a network to predict a subset of randomly sampled pixels from another subset of randomly sampled pixels [10]. Another adds yet more noise on top of the noisy input image [21, 22, 37]. These alterations encourage the network to instead learn a denoising function, but sacrifice valuable information contained in the noisy images to do so, limiting restoration quality.

Self-supervised denoisers have been adapted to structured noise in various ways. The works Structured Noise2Void (SN2V) [3] and MM-BSN [35] extended the blind-spot approach to also mask pixels containing noise that is correlated with the noise in the pixel being predicted. This approach can be conveniently applied directly to noisy data, provided that the extent of the noise correlations is known. However, it sacrifices even more information than before. Lee *et al.* [18] also extended the blind-spot approach, but by shuffling pixels to break up noise structures, making the noise effectively pixel-independent and ready

for traditional blind-spot denoising. This technique is however only applicable to relatively short range noise structures that might be found in consumer photography, not the longer range structures that are common in microscopy.

The technique of adding more noise [21, 22, 37] can be readily applied to structured noise, but an accurate noise model from which samples of noise can be quickly taken is needed. Training such a noise model for the extended structures that appear in some forms of scientific imaging is non-trivial.

2.2. Unsupervised denoising

Unlike self-supervised approaches, unsupervised approaches do not sacrifice information to enable denoising, but are instead limited by their dependence on a noise model. A noise model is a probability distribution over the noisy images that a camera system could produce when capturing a given signal, and is trained with suitable calibration data prior to denoising. Prakash *et al.* [24] first proposed using a noise model approximate the posterior – a probability distribution over the possible clean signals that could underlie a given noisy image, from which solutions can be randomly sampled. The noise model they used assumes noise is signal-dependent but unstructured. Salmon and Krull [27] later proposed using an autoregressive noise model to remove structured but signal-independent noise. Their method could also be applied to structured, signal-dependent noise, but it would be impractical, as the calibration data required to train a suitable noise model would also be suitable for training a traditional supervised denoiser.

Prakash *et al.* [23] proposed an improved VAE architecture for unsupervised denoising with a method called HDN. HDN was designed to tackle unstructured, signal-dependent noise, but the authors discovered that it could remove some cases of structured noise after a modification. Specifically, they prevented the network from reconstructing high-frequency content, thus removing high-frequency noise structures. This modified approach was called HDN₃₆.

3. Background

3.1. Image Formation and Denoising

We can express image formation as a two step process. The clean image, or as we also refer to it, the *signal*, \mathbf{s} , is drawn from a distribution $p(\mathbf{s})$ and then subjected to noise, producing the noisy image \mathbf{x} as drawn from the noise distribution $p(\mathbf{x}|\mathbf{s})$.

We assume that the noise distribution is centered around the signal, that is, the expected value of a noisy image equals the signal, $\mathbb{E}_{p(\mathbf{x}|\mathbf{s})}[\mathbf{x}] = \mathbf{s}$. In other words, the average of many noisy acquisitions will produce the clean image.

3.2. Variational Autoencoders

The following is a brief introduction to the deep learning framework our proposed denoiser is based upon, the Variational Autoencoder (VAE) [13]. For a more detailed tutorial, see [6]. Given observed variables \mathbf{x} , latent variables \mathbf{z} , prior distribution $p_\theta(\mathbf{z})$ and likelihood $p_\theta(\mathbf{x}|\mathbf{z})$, the VAE attempts to model \mathbf{x} by approximately minimizing this intractable objective,

$$\log p_\theta(\mathbf{x}) = \log \int p_\theta(\mathbf{x}|\mathbf{z})p_\theta(\mathbf{z})d\mathbf{z}, \quad (3)$$

with this tractable upper bound,

$$\begin{aligned} & \log p_\theta(\mathbf{x}) - D_{KL}[q_\phi(\mathbf{z}|\mathbf{x}) \parallel p_\theta(\mathbf{z}|\mathbf{x})] \\ & = \mathbb{E}_{q_\phi(\mathbf{z}|\mathbf{x})}[\log p_\theta(\mathbf{x}|\mathbf{z})] - D_{KL}[q_\phi(\mathbf{z}|\mathbf{x}) \parallel p_\theta(\mathbf{z})], \end{aligned} \quad (4)$$

where θ and ϕ are learnable parameters and D_{KL} is the Kullback-Leibler (KL) divergence [16]. Here, an approximate posterior $q_\phi(\mathbf{z}|\mathbf{x})$ is introduced and optimized to diverge as little as possible from the true posterior $p_\theta(\mathbf{z}|\mathbf{x})$.

The training process for this objective consists of first encoding an input \mathbf{x} as distribution $q_\phi(\mathbf{z}|\mathbf{x})$ over latent variables, then decoding a sample \mathbf{z} as distribution $p_\theta(\mathbf{x}|\mathbf{z})$ over images. The expectation of the likelihood is approximated with this single sample. The parameters θ and ϕ are adjusted to to maximise the log-likelihood of the input and to minimize the KL divergence between the approximate posterior and the prior. We refer to the former cost as the reconstruction error and the latter as the regularization error.

A common way to make a VAE more expressive is to make it hierarchical [28]. That is, using layers of latent variables, $\mathbf{z} = (\mathbf{z}_1, \mathbf{z}_2, \dots, \mathbf{z}_N)$, each conditionally dependent on the last. The prior and approximate posterior then factorize as

$$p_\theta(\mathbf{z}) = p_\theta(\mathbf{z}_1) \prod_{i=2}^N p_\theta(\mathbf{z}_i|\mathbf{z}_{i-1}) \quad (5)$$

$$q_\phi(\mathbf{z}|\mathbf{x}) = q_\phi(\mathbf{z}_1|\mathbf{x}) \prod_{i=2}^N q_\phi(\mathbf{z}_i|\mathbf{z}_{i-1}, \mathbf{x}). \quad (6)$$

3.3. PixelVAE

In the original formulation of the VAE, the decoding distribution $p_\theta(\mathbf{x}|\mathbf{z})$ was modeled as a diagonal Gaussian, where each element of \mathbf{x} is conditionally independent of all others. However, Gulrajani *et al.* [8] proposed using an AR distribution instead. In this approach, if the data are images, the distribution over each pixel is conditioned on “previous” pixels in a row-major order, as well as on \mathbf{z} . The decoding distribution can then be factorized as

$$p_\theta(\mathbf{x}|\mathbf{z}) = \prod_{i=1}^D p_\theta(x_i|x_{<i}, \mathbf{z}), \quad (7)$$

where D represents the number of pixels in the image, x_i represents the value of pixel i , and $x_{<i}$ represents the values of pixels preceding x_i . We refer to the set of pixels on which this distribution is conditioned as the decoder’s *receptive field*.

AR decoders are usually implemented by a convolutional neural network (CNN) with causal convolutions, which are convolutions whose kernel parameters are non-zero for only preceding pixels. [29, 30].

This modification is intended to make the VAE more expressive, but researchers and practitioners encountered an adverse effect of letting the receptive field include all valid pixels. They found that the decoder ignores \mathbf{z} and reconstructs the image using only the information available to it in $x_{<i}$. The regularization error would then drop to near zero, as the latent variable contains little to no information about \mathbf{x} , thus matching the prior, which contains absolutely no information about \mathbf{x} . This phenomenon is known as posterior collapse.

3.4. Variational Lossy Autoencoders

Chen *et al.* [4] investigated posterior collapse and found that it happens because, when $p_\theta(\mathbf{x}|\mathbf{z})$ is independent of \mathbf{z} , the true posterior becomes the prior. The approximate posterior then easily does the same, setting the regularization error to zero. They then go on to show that this does not only apply to the extreme case. The following is a brief interpretation of their findings.

In general, the regularization error is comparing the prior to the approximate posterior on how well it models the approximate posterior’s samples. The more \mathbf{x} affects the approximate posterior, the worse a model the \mathbf{x} -nescient prior will be. A VAE is therefore driven to minimize the representation of \mathbf{x} in its latent variables and instead model the data in its decoder.

Chen *et al.* demonstrated how this insight can be used to control the division of labour between the latent variable and the AR decoder. By limiting the receptive field in Eq. 7 to a small number of pixels in the neighborhood of x_i , the decoder learns to reconstruct fine-grained details without relying on \mathbf{z} , but has no choice other than to use \mathbf{z} for reconstructing global details. Consequently, only global information about \mathbf{x} is represented in the encoder’s latent variables.

4. Method

We use the findings in [4] to design a VAE-based model for removing signal-dependent, axis-aligned imaging noise.

We propose a restricted receptive field that gives an AR decoder all the information it needs to model the noise component of an image, but not enough information to model the signal. This will encourage an encoder to represent all the information about the signal in its latent variable \mathbf{z} , and

a paired decoder to describe the distribution of the noise, $p_\theta(\mathbf{x}|\mathbf{z}) \approx p(\mathbf{x}|\mathbf{s})$. We then propose a method for taking this code and mapping it back into pixel space to obtain a denoised estimate.

4.1. Autoregressive Receptive Fields and Noise

We expect an AR decoder with a receptive field that is too small to not model the noise, as it will not be able to capture all the occurring correlations. Conversely, a receptive field that is too large will start to model the signal, removing important information from the latent variable \mathbf{z} .

To design an appropriate receptive field, we must consider the types of structures that frequently occur in imaging noise. We find that many applications exhibit noise with an axis-aligned structure in only one direction. Figure 3 provides example scientific images with this type of noise structure, each accompanied by an autocorrelation plot of their noise.

These noise structures readily lend themselves to our approach when using a reduced receptive field that allows the decoder to look only up or left of the current position. It is unnecessary to include all correlated pixels, because at some point including more pixels will not add additional information about x_i , even if they are correlated with it. A experimental investigation of receptive field sizes can be found in Section 5.4.

Details on how we achieve this receptive field with our AR decoder architecture can be found in the supplementary material.

4.2. Decoding the Signal and Inference

Once our VAE has been trained, we have to extract an estimate of the signal for a noisy image. By feeding a noisy image \mathbf{x} into our encoder, a latent variable \mathbf{z} containing all the required information about our signal \mathbf{s} can be sampled. An additional network, termed *signal decoder*, is then used to convert that latent variable into an image. We train this signal decoder with training pairs $(\mathbf{z}^j, \mathbf{x}^j)$, where \mathbf{x}^j is a noisy training image and \mathbf{z}^j is the corresponding latent variable sampled from the encoding distribution $q_\phi(\mathbf{z}|\mathbf{x}^j)$. By relying on the assumption that the imaging noise is centered around the signal, we can train our decoder without clean data and use a quadratic Noise2Noise [19] training loss

$$\mathcal{L}(f_\nu(\mathbf{z}^j), \mathbf{x}^j) = |f(\mathbf{z}^j; \nu) - \mathbf{x}^j|^2, \quad (8)$$

where $f_\nu(\cdot)$ is the signal decoder with parameters ν .

Even though the signal decoder would naturally be trained in a second step after the main VAE is finished, in practice we co-trained it alongside the main VAE. At every training step, the sampled latent variable is fed to both decoders, but only the loss from the AR decoder is allowed to backpropagate to the encoder. This method of training is simply for convenience and we did not observe any changes

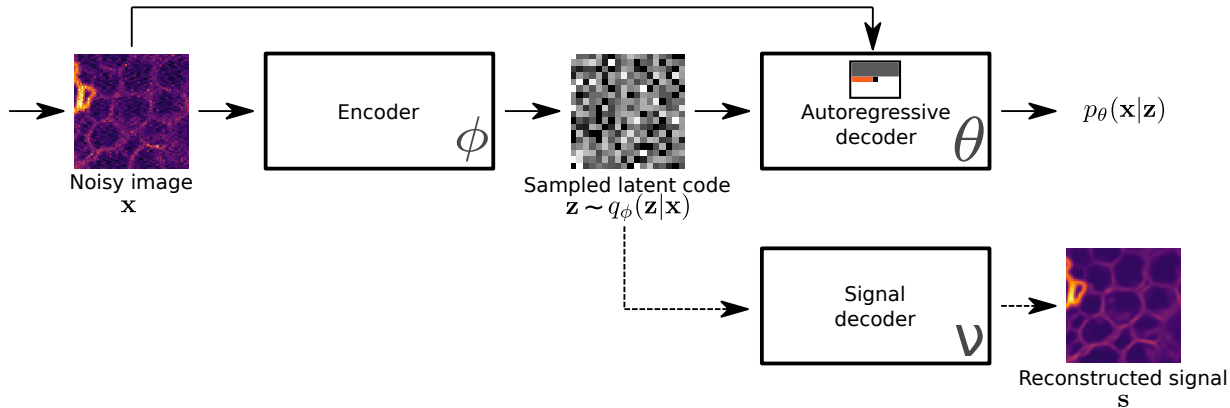


Figure 2. A Variational Lossy Autoencoder [4] (solid arrows) is trained to model the distribution of noisy images \mathbf{x} . The autoregressive decoder models the noise component of the images while the encoder models only the clean signal component \mathbf{s} . This behaviour is achieved by restricting the decoder’s receptive field. While a full autoregressive decoder is usually allowed to include pixels above and to the left (shown in grey and orange) our decoder includes only pixels in the same row as the pixel being modelled (shown in orange). This shows the decoder all that is needed to model row correlated noise but shows too little to model signal. The modification allows the encoder to capture only signal content in its latent variables \mathbf{z} . In a second step (dashed arrows), our novel *signal decoder* is trained to map latent variables into image space, revealing an estimate of the signal underlying \mathbf{x} . The training target for the signal decoder is simply the original noisy image.

in performance compared to a signal decoder that is trained separately, after the main VAE.

5. Experiments

5.1. Datasets

This section describes the 7 datasets that were used to test the performance of our proposed denoiser in comparison to three baselines.

The first four – *Convallaria A* [3], *Convallaria B* [25], *Mouse Actin* [25] and *Mouse Nuclei* [25], are from fluorescence microscopy, contain real noise and come with known ground truth. Three of these contain structured noise but the noise in *Mouse Nuclei* is unstructured. This unstructured dataset was included to demonstrate that the proposed method is still applicable to unstructured noise without modification, as an autoregressive decoder with the same receptive field as that used for the other three fluorescence microscopy datasets was used for *Mouse Nuclei*. It should also be noted that although *Convallaria B* [25] and *Mouse Actin* [25] were originally used to evaluate denoisers designed for unstructured noise, the autocorrelation plots in Figure 3 reveal structure. For details on dataset size and train/test splits, see each original publication.

Two datasets of natural images with simulated noise were also used. The Flickr Faces HQ thumbnails dataset [11], with resolution 128×128 , was made grayscale by averaging across color channels. For *FFHQ - Stripe*, the ground truth, \mathbf{s} , was scaled to have pixel values between 0 and 1, and Poisson noisy images were created as

$\mathbf{x} = 0.002 \times \mathcal{P}(\mathbf{s}/0.002)$. Zero-mean Gaussian noise with a standard deviation of 0.02 was then added to these images. Finally, structured noise was created by applying a horizontal Gaussian blur with a standard deviation of 1 to white Gaussian noise with a standard deviation of 0.025 and added on top.

For *FFHQ - Checkerboard*, we added noise with inverse signal dependence by sampling Gaussian noise from the distribution $\mathcal{N}(0, 0.15 \times 1/\mathbf{s})$. Then, a vertical checkerboard pattern was added by subtracting 0.1 from two pixels and adding 0.1 to the next two pixels along columns. The starting point for the checkerboard was randomly sampled from a uniform distribution. For both *FFHQ* datasets, the final 1000 images were designated as a testing set, and withheld from training the supervised denoiser CARE.

The last dataset used was *STEM*, a scanning transmission electron microscopy dataset from Henninen *et al.* [9], for which no ground truth is available.

5.2. Baselines

We compare the denoising performance of our method to three deep learning-based structured denoisers: the self-supervised denoiser Structured Noise2Void (SN2V) [3], the unsupervised denoiser Hierarchical DivNoising36 (HDN₃₆) [23] and the supervised denoiser Content Aware Image Restoration (CARE) [34].

The following are details on how each baseline is implemented in this paper, plus notes on our chosen architecture and AR receptive field design.

SN2V [3] must be adapted to each dataset by implement-

Table 1. Comparison with baseline methods using Peak Signal-to-Noise Ratio (PSNR). Higher is better. Best results are printed in **bold**. All datasets contain some form of structured noise, except for *Mouse Nuclei**. CARE is a supervised denoiser requiring examples of clean images, unlike the other baselines.

	SN2V	HDN	HDN ₃₆	HDN <i>large</i>	HDN ₃₆ <i>large</i>	Ours <i>small</i>	Ours <i>large</i>	CARE
Convallaria A	30.29	–	31.41	–	31.80	34.42	37.49	31.56
Convallaria B	31.67	37.39	37.21	–	37.92	38.99	44.10	36.71
Mouse Actin	32.80	34.12	–	–	34.14	36.50	39.23	34.20
Mouse Nuclei*	36.62	36.87	–	38.12	–	39.56	42.98	36.58
FFHQ - Stripe	29.52	–	32.64	–	34.54	32.87	35.66	36.46
FFHQ - Checkerboard	19.11	–	29.61	–	25.51	33.51	36.27	36.89

ing a mask that covers noise structures. Please refer to the supplementary to see how these masks were chosen for each dataset.

HDN₃₆ [23] requires a pixel-independent noise model,

$$p(\mathbf{x}|\mathbf{s}) = \prod_{i=1}^D p(x_i|s_i), \quad (9)$$

which we learnt as a Gaussian mixture model using the available ground truth high Signal-to-Noise Ratio (SNR) images. High-snr images were not available for the *STEM* dataset, so images denoised by our method were used as pseudo-ground truth. Since, like our method, this is VAE-based, it can produce infinitely many solutions. We follow Prakash *et al.* [23] and evaluate performance with the minimum mean square error (MMSE) estimate taken by averaging 100 samples.

Of the denoisers that do not require paired images, HDN₃₆'s performance is closest to ours, but the model implemented in the baseline publication uses significantly fewer parameters than ours (7 million to 25 million). We therefore additionally evaluate a version of HDN₃₆ with a similar number of parameters to ours, which was made by increasing the number of latent dimensions from 32 to 64. This model is referred to as HDN₃₆ *large*.

It should be noted that the *Convallaria B* and *Mouse Actin* datasets had been treated as unstructured by Prakash *et al.* [23] when testing the unstructured denoiser HDN. We additionally report those results in Table 5. It should also be noted that the noise in the *Mouse Nuclei* dataset is truly unstructured, so was denoised by HDN and its higher parameter version HDN *large*, which was made in the same way as HDN₃₆ *large*.

CARE, proposed by Weigert *et al.* [34], is a supervised approach that learns a mapping from low- to high-SNR images using example pairs. Therefore, unlike the other baselines and our method, it can only be applied to datasets with available ground truth. Furthermore, it cannot be evaluated on the images it was trained on, so the testing subset designated for each dataset was withheld from training this baseline model. Details of the train/test split for each dataset can

be found in Section 5.1.

Our Method requires a choice of orientation for the AR decoder's receptive field. As for SN2V, this was made using the spatial autocorrelation reported in Figure 3. Following the ablation study in Section 5.4, we always used a receptive field length of 40 pixels to the left of the pixel being predicted. For evaluation, we follow the same procedure as with HDN₃₆ [23] and average 100 solutions to produce an MMSE estimate.

Latent variables are produced by a fully convolutional hierarchical VAE [28], with 14 levels to its hierarchy. We note that our model requires almost 20GB of GPU memory to train, which is impractical for many users, so additionally evaluate a reduced version that requires approximately 6GB of GPU memory to train. This was made by reducing the number of latent variables from 14 to 6. We refer to these models as Ours *small* and Ours *large*, for the lower memory and higher memory versions respectively. See the supplementary materials for full architecture and training details.

5.3. Comparing Denoising Performance

Quantitative results measured in Peak Signal-to-Noise Ratio (PSNR) are reported in Table 5. Note that HDN₃₆ failed to train with the *Mouse Actin* dataset. Out of the methods that do not require clean images, Ours *large* achieved the highest PSNR across all datasets, even beating the supervised CARE on the four microscopy datasets. Ours *small* then had the second highest PSNR on all datasets except FFHQ - *Stripe*, where it was beaten by HDN₃₆ *large*, although it should be noted that HDN₃₆ *large* requires almost 20GB of GPU memory to train while Ours *small* requires only 6GB.

Looking at the qualitative results in Fig. 3, we see that Ours *large* denoised images from each dataset without leaving behind any artifacts, whereas HDN₃₆ *large* could not remove the structured component of the noise from the FFHQ - *Checkerboard* or the *STEM* dataset. SN2V left artifacts on all datasets with structured noise, but not for the unstructured *Mouse Nuclei* dataset. It can also be seen that Ours *large* produced the sharpest and most accurate images.

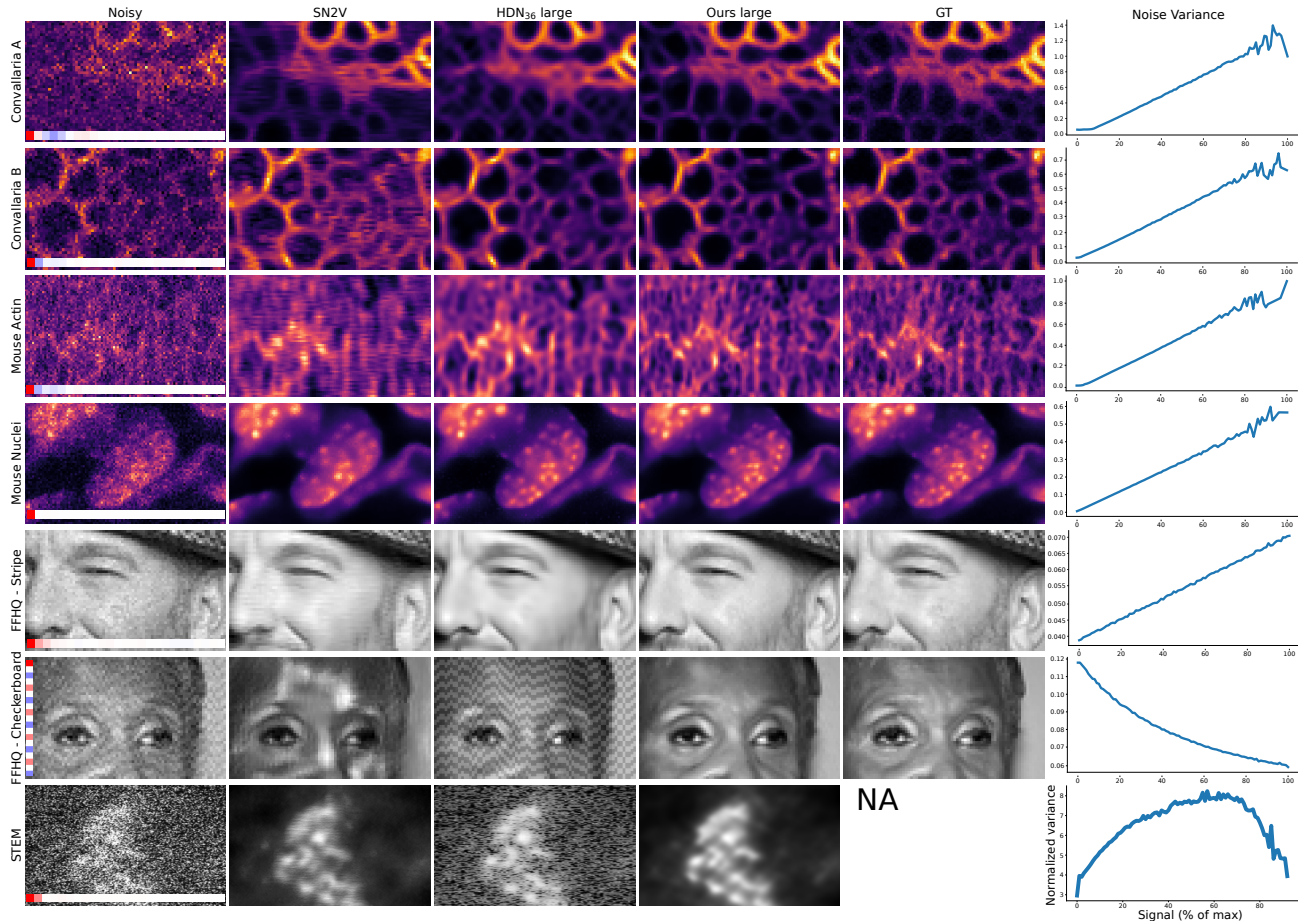


Figure 3. Visual results from our method and the two baselines on all datasets, including the qualitative *STEM* dataset for which no ground truth was available. The spatial autocorrelation of the noise is overlaid on each noisy image, with red indicating positive correlation and blue indicating negative correlation. The direction of the correlation is given by the orientation of the autocorrelation bar. Additionally, the signal dependence of each dataset is shown in the graphs in the right-hand column. On the horizontal axis of these graphs is the clean signal intensity as a percentage of the maximum, while on the vertical axis is the variance of noisy pixel values recorded for these signal intensities.

5.4. Ablation Study - Receptive Field Size

As stated in Section 4, to model the noise structures addressed in this paper, a VAE’s AR decoder’s receptive field must span pixels in the same row or column as the pixel being modelled. The number of pixels spanned must also be determined. To investigate receptive field size, we denoised the *FFHQ - Checkerboard* dataset using a range of RF sizes, from 10 pixels to 120 pixels, and measured the effect on PSNR. The results of this study are reported in Figure 4.

The study shows that the AR decoder is able to model this structured noise, and therefore have the noise removed by the encoder, when the receptive field spans 40 pixels. PSNR drops by 0.06 when the receptive field reaches 80 pixels, and rises by 0.03 when at 120 pixels. If we assume that these relatively small changes are only due to random

variations in training, we can also draw the conclusion that more of the underlying signal is not modelled by the AR decoder as the receptive field grows. Following the results of this ablation study, the receptive field of all models trained to denoise in Section 5.3 are set to span 40 pixels.

5.5. Ablation Study - Noise Reconstruction

If the VAE’s decoder is modelling only the noise component of images, encoding an image with the VAE and sampling from the AR decoder should yield an image with the same underlying signal but a different random sample of noise. If the decoder’s model of the noise is accurate, the sampled noise should exhibit the same autocorrelation and signal-dependence characteristics as the noise in the original image. An investigation into this is reported in Figure 5, where a noisy image from the *Convallaria A* dataset was

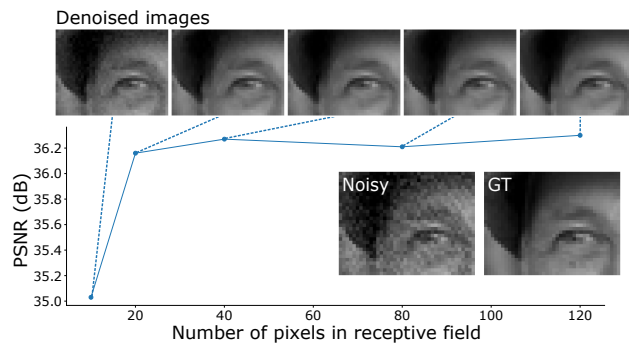


Figure 4. After determining the direction for the AR decoder’s receptive field, the extent of it must be decided. Here, we denoised the *FFHQ - Checkerboard* dataset 5 times, varying the number of pixels covered by the AR decoder’s receptive field. The PSNR of images denoised by each model was then calculated. Images show denoising results for different receptive field sizes.

encoded by a trained VAE, with a latent variable sampled and used by the VAE’s AR decoder to sample a reconstruction of the original image. The reconstructed noise exhibits spatial autocorrelation and signal dependence very similar to the real noise, indicating that our AR decoder has learnt an accurate model of the noise.

6. Conclusion

We proposed a unsupervised VAE-based denoising algorithm for structured and signal-dependent noise that is inspired by Variational Lossy Autoencoders. By engineering the receptive field of the AR decoder, we were able to encourage the VAE’s latent variables to represent the signal content of an image while discarding the noise. We also presented a novel signal decoder that is then trained to map this latent variable into an estimate of the clean image.

The algorithm outperforms both the self-supervised denoiser SN2V [3] and the unsupervised denoiser HDN₃₆ [23] on all tests. It also outperforms the supervised denoiser CARE [34] on 4 of 6 datasets.

The algorithm is suited to noise with correlations that run parallel to the axes of the image. Such noise commonly occurs in a plethora of scientific imaging settings, such as microscopy or astronomy. Often, users in labs around the world are unable to find suitable unsupervised methods to remove such noise. We release our code as open source and strongly believe that the scientific imaging community will apply and adapt our methods in a variety of applications.

While we have achieved our results using simple 1-dimensional receptive fields, some imaging modalities produce noise that is correlated in multiple directions, therefore requiring a differently shaped receptive field. We found that extending the receptive field to cover both a row and column of pixels allows the decoder to model some aspects of

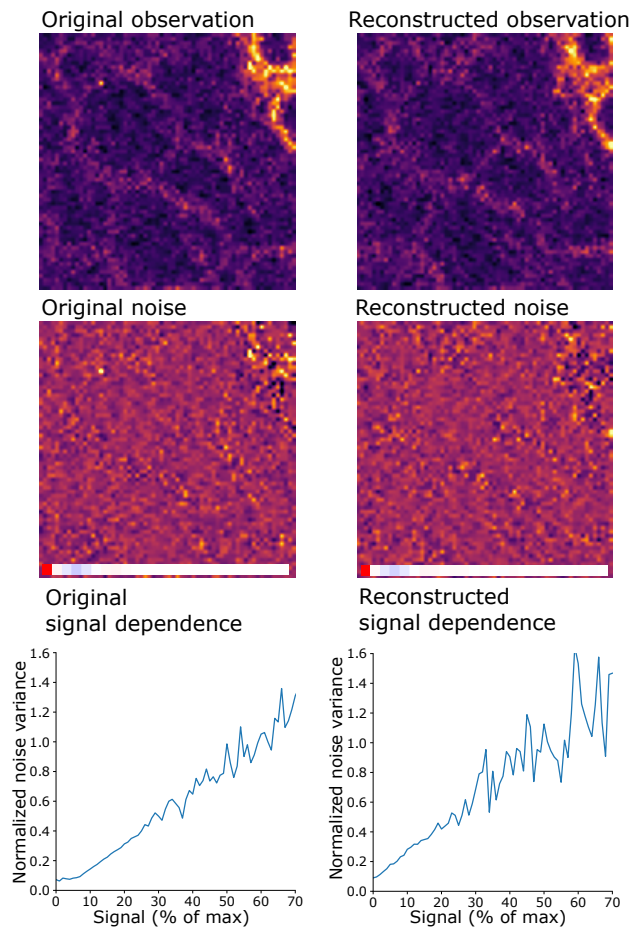


Figure 5. A noisy image from the *Convallaria A* dataset was encoded by a trained VAE and a sample from the VAE’s autoregressive (AR) decoder was taken. The reconstructed observation has the same underlying signal as the original but a new sample of noise. Here, we examine this sampled noise to check that its spatial autocorrelation and signal dependence match those of the real noise, indicating that the AR decoder accurately models the noise.

the signal, making the technique unsuitable for removing noise correlated in two dimensions. However, we believe that techniques other than shaping the AR decoder receptive field could be discovered to limit the decoder’s modelling capabilities. We hope that future work will further improve the theoretical understanding of the method and allow us to utilize its full potential.

Acknowledgements

The computations described in this paper were performed using the University of Birmingham’s BlueBEAR HPC service, which provides a High Performance Computing service to the University’s research community. See <http://www.birmingham.ac.uk/bear> for more details.

References

- [1] European Machine Vision Association. Emva standard 1288: Standard for characterization of image sensors and cameras. *EMVA 1288*, 2010. [2](#)
- [2] Joshua Batson and Loic Royer. Noise2self: Blind denoising by self-supervision. In *International Conference on Machine Learning*, pages 524–533. PMLR, 2019. [1](#), [2](#)
- [3] Coleman Broaddus, Alexander Krull, Martin Weigert, Uwe Schmidt, and Gene Myers. Removing structured noise with self-supervised blind-spot networks. In *2020 IEEE 17th International Symposium on Biomedical Imaging (ISBI)*, pages 159–163. IEEE, 2020. [2](#), [5](#), [8](#)
- [4] Xi Chen, Diederik P Kingma, Tim Salimans, Yan Duan, Prfulla Dhariwal, John Schulman, Ilya Sutskever, and Pieter Abbeel. Variational lossy autoencoder. In *International Conference on Learning Representations*, 2017. [2](#), [4](#), [5](#)
- [5] Kostadin Dabov, Alessandro Foi, Vladimir Katkovnik, and Karen Egiazarian. Image denoising with block-matching and 3d filtering. In *Image processing: algorithms and systems, neural networks, and machine learning*, volume 6064, pages 354–365. SPIE, 2006. [1](#), [2](#)
- [6] Carl Doersch. Tutorial on variational autoencoders. *arXiv e-prints*, pages arXiv–1606, 2016. [3](#)
- [7] Shuhang Gu, Lei Zhang, Wangmeng Zuo, and Xiangchu Feng. Weighted nuclear norm minimization with application to image denoising. In *Proceedings of the IEEE conference on computer vision and pattern recognition*, pages 2862–2869, 2014. [2](#)
- [8] Ishaan Gulrajani, Kundan Kumar, Faruk Ahmed, Adrien Ali Taiga, Francesco Visin, David Vazquez, and Aaron Courville. Pixelvae: A latent variable model for natural images. *arXiv preprint arXiv:1611.05013*, 2016. [3](#)
- [9] Trond R Henninen, Marta Bon, Feng Wang, Daniele Passerone, and Rolf Erni. The structure of sub-nm platinum clusters at elevated temperatures. *Angewandte Chemie International Edition*, 59(2):839–845, 2020. [5](#)
- [10] Tao Huang, Songjiang Li, Xu Jia, Huchuan Lu, and Jianzhuang Liu. Neighbor2neighbor: Self-supervised denoising from single noisy images. In *Proceedings of the IEEE/CVF conference on computer vision and pattern recognition*, pages 14781–14790, 2021. [1](#), [2](#)
- [11] Tero Karras, Samuli Laine, and Timo Aila. A style-based generator architecture for generative adversarial networks. In *Proceedings of the IEEE/CVF conference on computer vision and pattern recognition*, pages 4401–4410, 2019. [5](#)
- [12] Amirhossein Khalilian-Gourtani, Mariano Tepper, Victor Minden, and Dmitri B Chklovskii. Strip the stripes: artifact detection and removal for scanning electron microscopy imaging. In *ICASSP 2019-2019 IEEE International Conference on Acoustics, Speech and Signal Processing (ICASSP)*, pages 1060–1064. IEEE, 2019. [2](#)
- [13] Diederik P Kingma and Max Welling. Auto-encoding variational bayes. *stat*, 1050:1, 2014. [3](#)
- [14] Alexander Krull, Tim-Oliver Buchholz, and Florian Jug. Noise2void-learning denoising from single noisy images. In *Proceedings of the IEEE/CVF conference on computer vision and pattern recognition*, pages 2129–2137, 2019. [1](#), [2](#)
- [15] Alexander Krull, Tomáš Vičar, Mangal Prakash, Manan Lalit, and Florian Jug. Probabilistic noise2void: Unsupervised content-aware denoising. *Frontiers in Computer Science*, 2:5, 2020. [1](#), [2](#)
- [16] Solomon Kullback and Richard A Leibler. On information and sufficiency. *The annals of mathematical statistics*, 22(1):79–86, 1951. [3](#)
- [17] Romain F Laine, Guillaume Jacquemet, and Alexander Krull. Imaging in focus: an introduction to denoising bioimages in the era of deep learning. *The international journal of biochemistry & cell biology*, 140:106077, 2021. [1](#), [2](#)
- [18] Wooseok Lee, Sanghyun Son, and Kyoung Mu Lee. Apbsn: Self-supervised denoising for real-world images via asymmetric pd and blind-spot network. In *Proceedings of the IEEE/CVF Conference on Computer Vision and Pattern Recognition*, pages 17725–17734, 2022. [2](#)
- [19] Jaakko Lehtinen, Jacob Munkberg, Jon Hasselgren, Samuli Laine, Tero Karras, Miika Aittala, and Timo Aila. Noise2noise: Learning image restoration without clean data. In *International Conference on Machine Learning*, pages 2965–2974. PMLR, 2018. [2](#), [4](#)
- [20] Yu Liu, Kurt Weiss, Nassir Navab, Carsten Marr, Jan Huiskens, and Tingying Peng. Destripe: A self2self spatio-spectral graph neural network with unfolded hessian for stripe artifact removal in light-sheet microscopy. In *Medical Image Computing and Computer Assisted Intervention–MICCAI 2022: 25th International Conference, Singapore, September 18–22, 2022, Proceedings, Part IV*, pages 99–108. Springer, 2022. [2](#)
- [21] Nick Moran, Dan Schmidt, Yu Zhong, and Patrick Coady. Noisier2noise: Learning to denoise from unpaired noisy data. In *Proceedings of the IEEE/CVF Conference on Computer Vision and Pattern Recognition*, pages 12064–12072, 2020. [2](#), [3](#)
- [22] Tongyao Pang, Huan Zheng, Yuhui Quan, and Hui Ji. Recorrupted-to-recorrupted: Unsupervised deep learning for image denoising. In *Proceedings of the IEEE/CVF conference on computer vision and pattern recognition*, pages 2043–2052, 2021. [2](#), [3](#)
- [23] Mangal Prakash, Mauricio Delbracio, Peyman Milanfar, and Florian Jug. Interpretable unsupervised diversity denoising and artefact removal. In *International Conference on Learning Representations*, 2021. [1](#), [3](#), [5](#), [6](#), [8](#)
- [24] Mangal Prakash, Alexander Krull, and Florian Jug. Fully unsupervised diversity denoising with convolutional variational autoencoders. *arXiv preprint arXiv:2006.06072*, 2020. [1](#), [2](#), [3](#)
- [25] Mangal Prakash, Manan Lalit, Pavel Tomancak, Alexander Krull, and Florian Jug. Fully unsupervised probabilistic noise2void. In *2020 IEEE 17th International Symposium on Biomedical Imaging (ISBI)*, pages 154–158. IEEE, 2020. [5](#)
- [26] Yuhui Quan, Mingqin Chen, Tongyao Pang, and Hui Ji. Self2self with dropout: Learning self-supervised denoising from single image. In *Proceedings of the IEEE/CVF conference on computer vision and pattern recognition*, pages 1890–1898, 2020. [1](#)
- [27] Benjamin Salmon and Alexander Krull. Towards structured noise models for unsupervised denoising. In *European Con-*

- ference on Computer Vision*, pages 379–394. Springer, 2022. [2](#), [3](#)
- [28] Casper Kaae Sønderby, Tapani Raiko, Lars Maaløe, Søren Kaae Sønderby, and Ole Winther. Ladder variational autoencoders. *Advances in neural information processing systems*, 29, 2016. [3](#), [6](#)
- [29] Aaron Van den Oord, Nal Kalchbrenner, Lasse Espeholt, Oriol Vinyals, Alex Graves, et al. Conditional image generation with pixelcnn decoders. *Advances in neural information processing systems*, 29, 2016. [4](#)
- [30] Aaron Van Oord, Nal Kalchbrenner, and Koray Kavukcuoglu. Pixel recurrent neural networks. In *International conference on machine learning*, pages 1747–1756. PMLR, 2016. [4](#)
- [31] Ende Wang, Ping Jiang, Xuepeng Li, and Hui Cao. Infrared stripe correction algorithm based on wavelet decomposition and total variation-guided filtering. *journal of the european optical society-rapid publications*, 16:1–12, 2020. [2](#)
- [32] Feng Wang, Trond R Henninen, Debora Keller, and Rolf Erni. Noise2atom: unsupervised denoising for scanning transmission electron microscopy images. *Applied Microscopy*, 50(1):1–9, 2020. [2](#)
- [33] Zejin Wang, Jiazheng Liu, Guoqing Li, and Hua Han. Blind2unblind: Self-supervised image denoising with visible blind spots. In *Proceedings of the IEEE/CVF Conference on Computer Vision and Pattern Recognition*, pages 2027–2036, 2022. [2](#)
- [34] Martin Weigert, Uwe Schmidt, Tobias Boothe, Andreas Müller, Alexandr Dibrov, Akanksha Jain, Benjamin Wilhelm, Deborah Schmidt, Coleman Broaddus, Siân Culley, et al. Content-aware image restoration: pushing the limits of fluorescence microscopy. *Nature methods*, 15(12):1090–1097, 2018. [1](#), [2](#), [5](#), [6](#), [8](#)
- [35] Dan Zhang, Fangfang Zhou, Yuwen Jiang, and Zhengming Fu. Mm-bsn: Self-supervised image denoising for real-world with multi-mask based on blind-spot network. In *Proceedings of the IEEE/CVF Conference on Computer Vision and Pattern Recognition*, pages 4188–4197, 2023. [2](#)
- [36] Kai Zhang, Wangmeng Zuo, Yunjin Chen, Deyu Meng, and Lei Zhang. Beyond a gaussian denoiser: Residual learning of deep cnn for image denoising. *IEEE transactions on image processing*, 26(7):3142–3155, 2017. [2](#)
- [37] Yi Zhang, Dasong Li, Ka Lung Law, Xiaogang Wang, Hongwei Qin, and Hongsheng Li. Idr: Self-supervised image denoising via iterative data refinement. In *Proceedings of the IEEE/CVF Conference on Computer Vision and Pattern Recognition*, pages 2098–2107, 2022. [2](#), [3](#)
- [38] Yide Zhang, Yinhao Zhu, Evan Nichols, Qingfei Wang, Siyuan Zhang, Cody Smith, and Scott Howard. A poisson-gaussian denoising dataset with real fluorescence microscopy images. In *CVPR*, 2019. [2](#)

Unsupervised Structured Noise Removal with Variational Lossy Autoencoder - Supplementary

Benjamin Salmon and Alexander Krull

School of Computer, University of Birmingham, Birmingham B15 2TT, UK

brs209@student.bham.ac.uk, a.f.f.krull@bham.ac.uk

1. Technical details

1.1. Network architecture

We proposed two network architectures for denoising, one *large* and one *small*. Each model consists of a hierarchical Variational Autoencoder (VAE) [6], an autoregressive decoder [8] and our novel *signal decoder*. In the *large* network, the VAE has 14 levels to its hierarchy. The first 13 levels have 64 latent dimensions each, while the final level has 128 dimensions. The latent variable passed to the decoders is sampled from this final level. At each level on both the bottom-up path and the top-down path is a residual block consisting of two sets of a convolution followed by a batch normalization [3] followed by a Mish activation function [5]. Each residual block is followed by a gated block [7]. Resampling is performed at every other level.

The *small* network was the same except for having 6 levels to its hierarchy and half the latent dimensions.

The autoregressive decoder is built with 8 layers of residual causal convolution blocks similar to those proposed in [8], but we found performance to be better with a ReLU activation function [1] than the gated units. Convolutions at every other layer have dilated kernels [9] and all have 64 filters. The likelihood distribution is a Gaussian mixture model, with 3 components used for all datasets except the *FFHQ* datasets, for which 10 were used, and the *STEM* dataset, for which 5 were used.

The *signal decoder* is a convolutional neural network consisting of 4 convolutions with 128 filters, each followed by a ReLU activation function.

1.2. Training

Both the main VAE and signal decoder were trained with an Adamax [4] optimizer with a learning rate of 0.002. Both learning rates decreased by a factor of 10 when validation loss had plateaued for 50 epochs. Models for all datasets were trained for a maximum of 80,000 steps, which took approximately 24 hours, but stopped if validation loss had plateaued for 100 epochs.

For the microscopy datasets, training images were randomly cropped to a size of 256×256 at each epoch and batch size of 16 was used, but this was split into 4 virtual batches. For the *FFHQ - Stripe* and *FFHQ - Checkerboard* datasets, training images were kept at their original resolution of 128×128 and a batch size of 64 was used, but split into 16 virtual batches. For all datasets, training required approximately 20GB of GPU memory with the *large* network and 6GB with the *small* network.

1.3. SN2V masks

Following Broaddus *et al.* [2], self-supervised denoising masks should be as small as possible while covering pixels with a noise value that is highly predictive of the noise in the target pixel. A trial and error test of mask size for each dataset would be too computationally expensive, so we follow [2] and mask 4 pixels on each side of the target pixel for *Convallaria A*, *Convallaria B*, *Mouse Actin*, *STEM* and *FFHQ - Stripe*. The structured component of noise in the *FFHQ - Checkerboard* dataset can theoretically be predicted by seeing only two pixels in the same column, so entire columns were masked here. The orientation of the pixel mask was determined by looking at the spatial autocorrelation in noise patches for each dataset. The *Mouse Nuclei* dataset is corrupted by unstructured noise, so was denoised with a single pixel mask.

2. Additional qualitative results

Please see overleaf for larger denoised images from each dataset.

References

- [1] Abien Fred Agarap. Deep learning using rectified linear units (relu). *arXiv preprint arXiv:1803.08375*, 2018.
- [2] Coleman Broaddus, Alexander Krull, Martin Weigert, Uwe Schmidt, and Gene Myers. Removing structured noise with self-supervised blind-spot networks. In *2020 IEEE 17th International Symposium on Biomedical Imaging (ISBI)*, pages 159–163. IEEE, 2020.

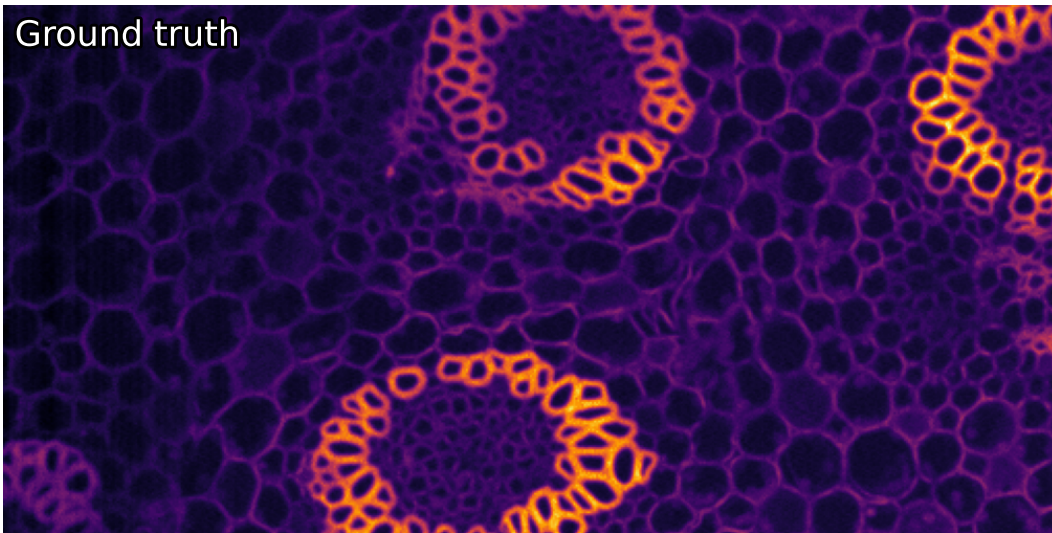
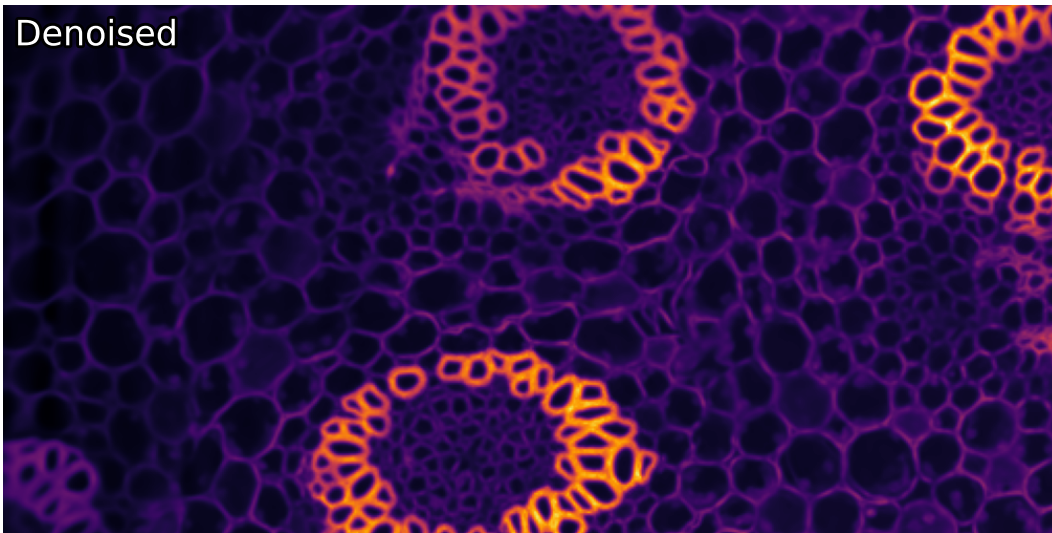
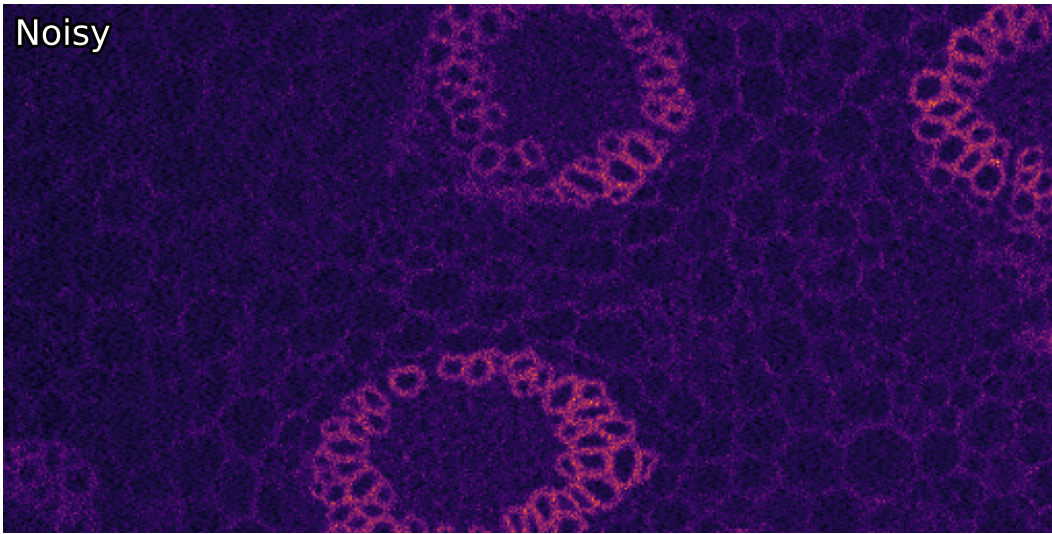


Figure 1. *Convallaria A*

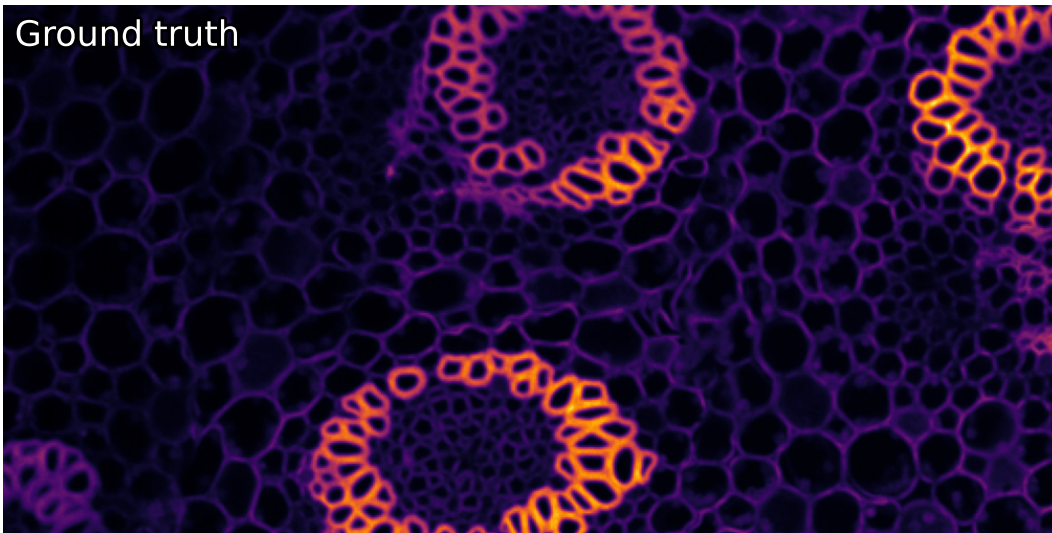
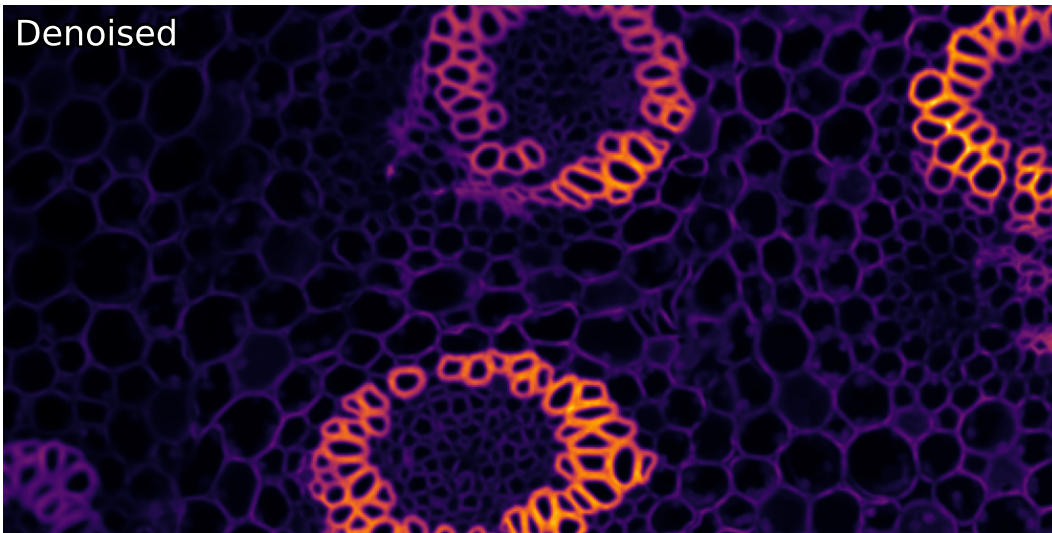
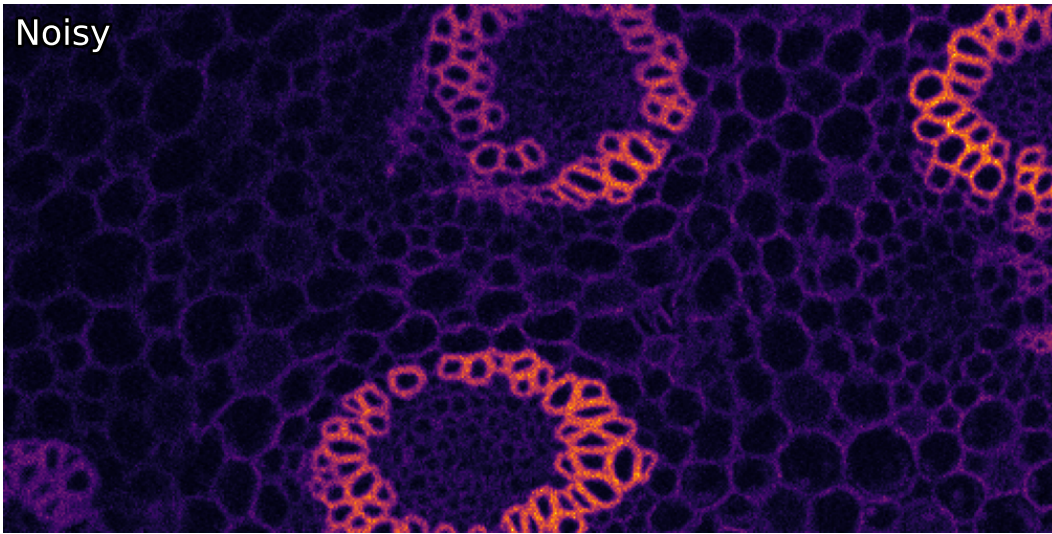


Figure 2. *Convallaria B*

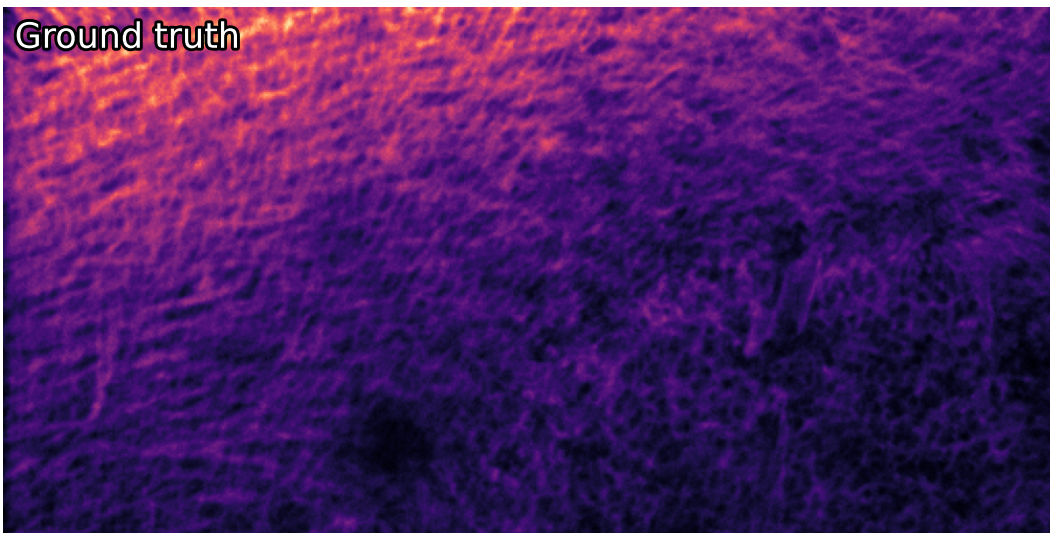
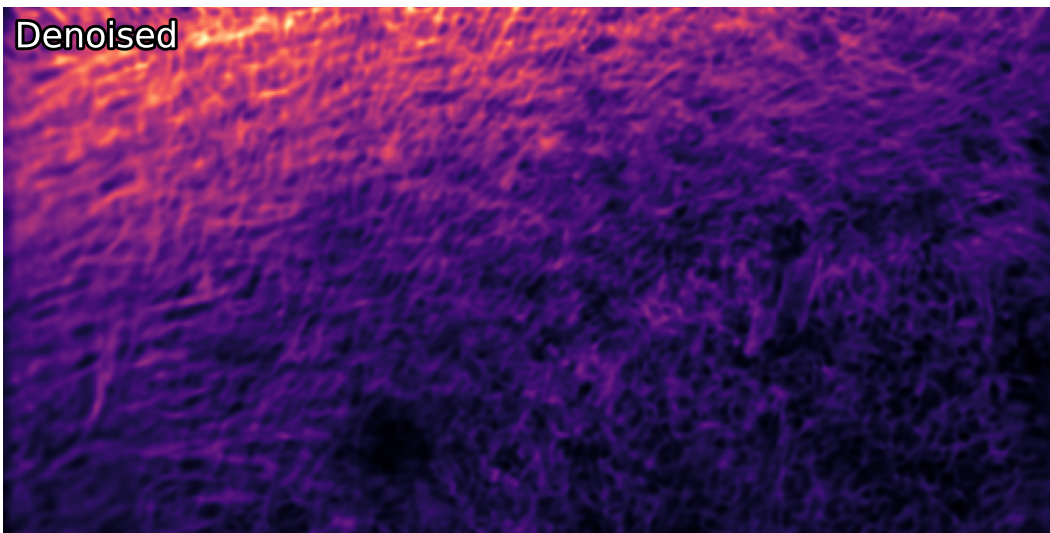
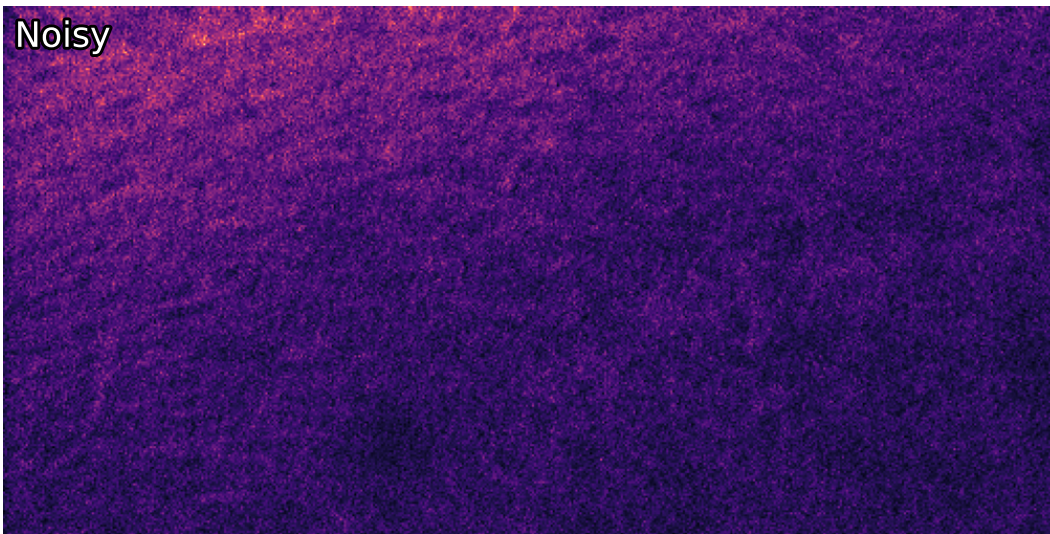


Figure 3. *Mouse Actin*

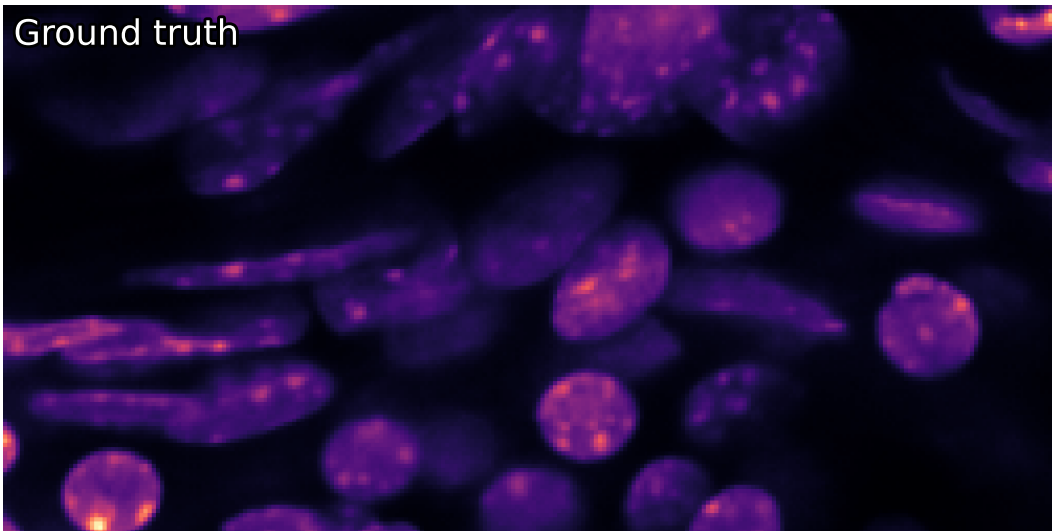
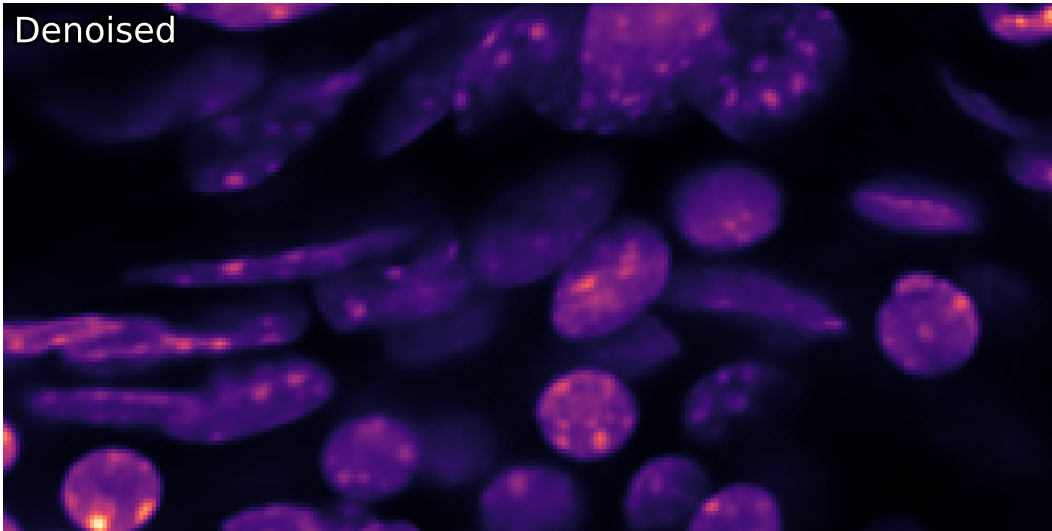
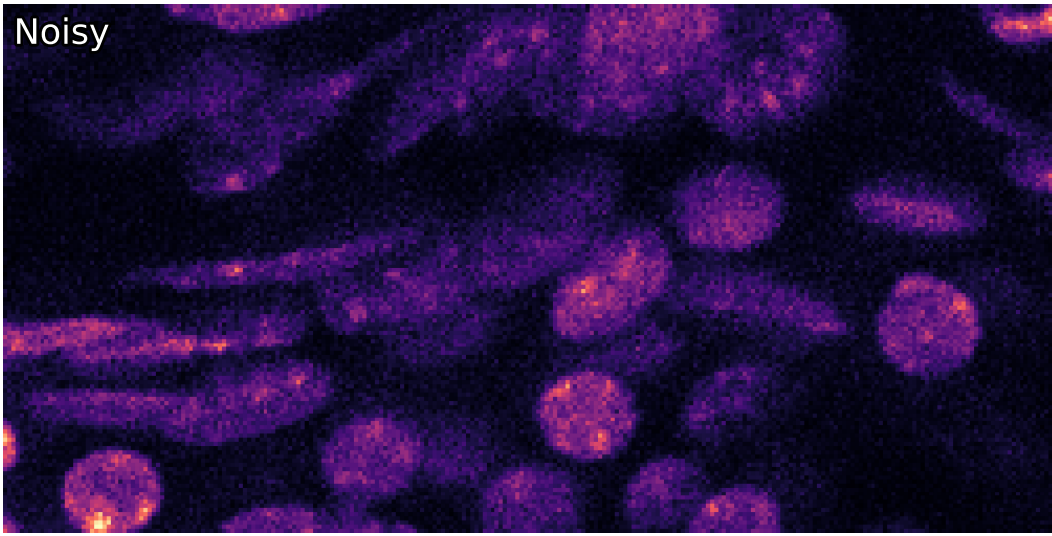


Figure 4. *Mouse Nuclei*



Figure 5. *FFHQ - Stripe*



Figure 6. *FFHQ - Checkerboard*

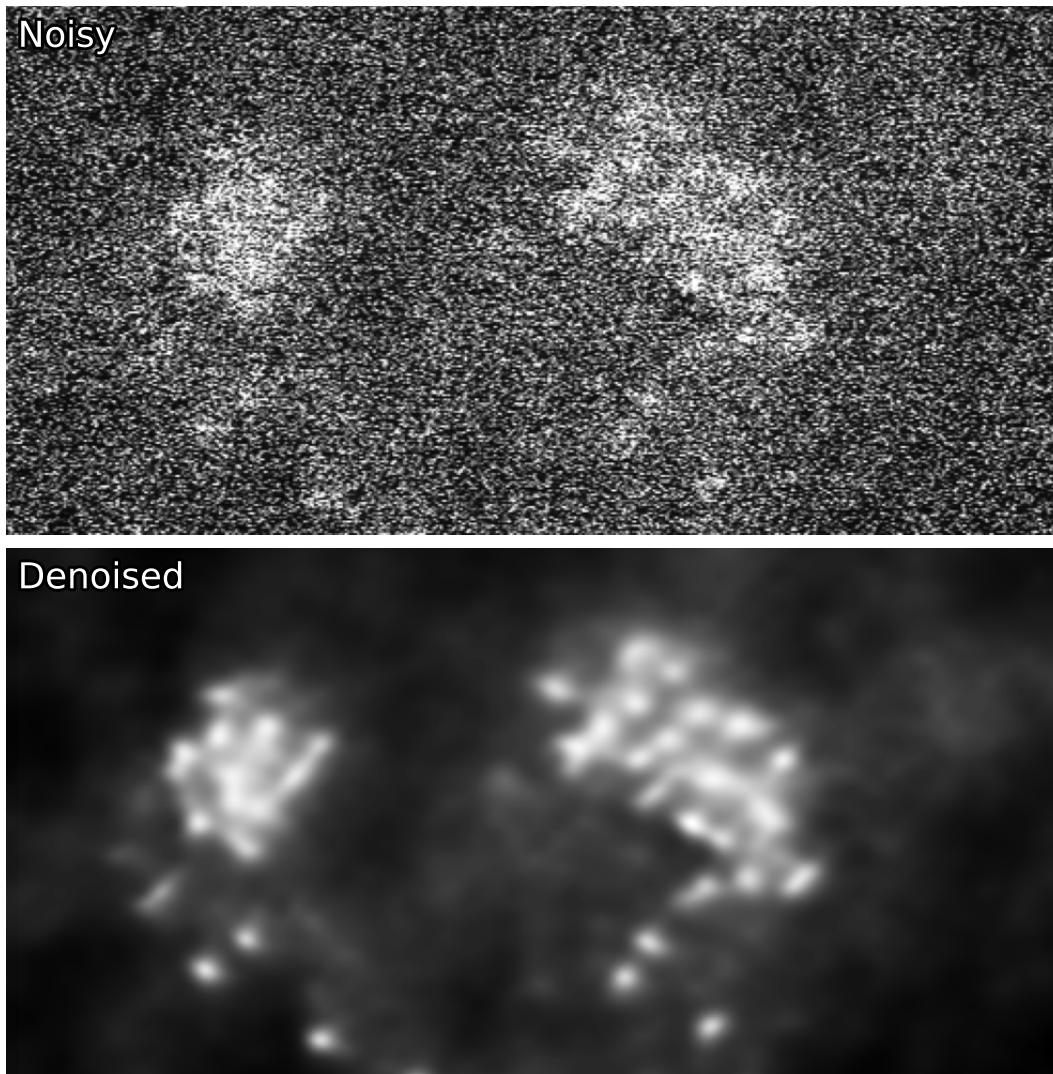


Figure 7. *STEM*

- [3] Sergey Ioffe and Christian Szegedy. Batch normalization: Accelerating deep network training by reducing internal covariate shift. In *International conference on machine learning*, pages 448–456. pmlr, 2015.
- [4] Diederik P Kingma and Jimmy Ba. Adam: A method for stochastic optimization. *arXiv preprint arXiv:1412.6980*, 2014.
- [5] Diganta Misra. Mish: A self regularized non-monotonic activation function. *arXiv preprint arXiv:1908.08681*, 2019.
- [6] Casper Kaae Sønderby, Tapani Raiko, Lars Maaløe, Søren Kaae Sønderby, and Ole Winther. Ladder variational autoencoders. *Advances in neural information processing systems*, 29, 2016.
- [7] Arash Vahdat and Jan Kautz. Nvae: A deep hierarchical variational autoencoder. *Advances in neural information processing systems*, 33:19667–19679, 2020.
- [8] Aaron Van den Oord, Nal Kalchbrenner, Lasse Espeholt, Oriol Vinyals, Alex Graves, et al. Conditional image generation with pixelcnn decoders. *Advances in neural information processing systems*, 29, 2016.
- [9] Fisher Yu and Vladlen Koltun. Multi-scale context aggregation by dilated convolutions. *arXiv preprint arXiv:1511.07122*, 2015.